ADVANCED MATERIALS INTERFACES
www.advmatinterfaces.de

Restructuring and Reshaping of $CsPbX_3$ Perovskites by Lithium Salts

*Antoine Dumont, Eric Nicholson, Chenyue Qiu, Jinbo Pan, Zachary Gariepy, Shixuan Du, Jane Howe, Chandra Veer Singh, and Zheng-Hong Lu**

Metal halide perovskites have exceptional potential for future generations of light-emitting diodes and solar cells. Compared to widely used solution-based syntheses, vapor-phase deposition (VPD) offers a fabrication route that can be more easily scaled up for commercial production. Cesium lead halides ($CsPbX_3$) have shown great color purity, high photoluminescence quantum yield, and better stability than other perovskites. To improve the optoelectronic properties, lithium salts are often used as passivation agents to reduce nonradiative defects. Here, it is reported that VPD $CsPbX_3$ thin films can be dramatically reshaped by a lithium bromide adlayer, a salt that is successfully used to drastically increase the luminescent yield of $CsPbBr_3$. It is found that continuous $CsPbBr_3$ and $CsPbCl_3$ films restructure themselves into islands whereas $CsPbI_3$ films transform into mixed triangular and rod-shaped crystals. Based on density functional theory (DFT) studies, it is established that a surface energy change by LiBr adlayer is not the main driver for the perovskite film transformation. Instead, DFT simulations indicate that the LiBr adlayer creates a polar surface forming a strong Van der Waals force attracting water molecules.

1. Introduction

Perovskite materials are now one of the main focuses of photovoltaic and optoelectronic devices due to their high appeal of simple synthesis and sky-rocketing efficiency. Perovskites also can have an easily tunable bandgap when changing or combining halide anions with a narrow emission and have often demonstrated near-unity photoluminescence quantum yield (PLQY).[1,2] Operational stability has been a major issue for perovskite devices. Inorganic lead halide perovskites have been showing a significant performance increase in the last decade for both solar cells and light emitting diodes (LED), partly due to their higher tolerance to ambient atmosphere and moisture compared to organic-inorganic hybrid perovskites.[3,4] Traditionally, perovskites have mainly been studied using solution-processing methods due to their facile synthesis. In contrast, vapor-phase deposition (VPD) in vacuum offers a safe environment for crystal growth and the essential easy scalability for industrial production of perovskite optoelectronics which is severely limited for solution-processed devices.[5–7] All-inorganic perovskites are also easier to fabricate in vacuum due to their precursors' lower volatility compared to organic salts which can be detrimental to the system's pressure. The performances of VPD perovskite devices are still lacking compared to records attained with solution-based films, but the perovskite growth through VPD is fundamentally different from solution methods. Understanding the behavior of perovskite thin films fabricated through VPD and how it differs from solution-processed ones is critical to improve device performance and stability. Pin-holes, mechanical stress, and localized crystalline phase change can drastically lower efficiency by lowering exciton recombination rate or creating nonradiative recombination for LED.[8,9] More studies on the deposition process optimization and passivation of nonradiative defects through buffer or capping layers are essential to improve the challenging low PLQY of VPD perovskite films.

The nature of the passivation used can strongly affect the PLQY of perovskites. VPD does not allow the use of large organic ligands that have been very successful in improving perovskite performance in the last decade. Inorganic salts or LiBr addition to $CsPbBr_3$ vapor-deposited films was previously demonstrated to have a drastic improvement to the brightness of the perovskite films and the overall performance of LED devices[10] as well as an astonishing restructuring and reshaping of the thin film morphology.[11] There are still questions related to the fundamental reasons why this phenomenon occurs, and this paper attempts to bring some answers. Looking at the $CsPbX_3$ (X = Br, Cl, I) family and how they react to the lithium salt, we aimed to determine the material science behind the self-assembly behavior. In this work, we studied

A. Dumont, E. Nicholson, C. Qiu, Z. Gariepy, J. Howe, C. V. Singh, Z.-H. Lu
Department of Materials Science and Engineering
University of Toronto
Toronto M5S3E5, Canada
E-mail: zhenghong.lu@utoronto.ca
J. Pan, S. Du
Nanoscale Physics and Devices Laboratory
Institute of Physics
Chinese Academy of Sciences
NanSanJie 8, ZhongGuanCun, Beijing 100190, China

The ORCID identification number(s) for the author(s) of this article can be found under https://doi.org/10.1002/admi.202201296.

DOI: 10.1002/admi.202201296

the structural and morphological changes in $CsPbX_3$ films and compare their behavior when passivated with LiBr using scanning electron microscopy (SEM), X-ray diffraction (XRD), and scanning/transmission electron microscopy (S/TEM). The $CsPbBr_3$ and $CsPbCl_3$ show similar restructuration from thin film to spherical islands, but $CsPbI_3$ is unique with its triangular and rod-shaped nanostructures. Variations in crystal structure are identified using TEM. The morphological transformation process is studied by imaging of the impact of an increasing input of LiBr or an increasing perovskite thickness. Atmospheric exposure to moisture is found to create a similar behavior as LiBr but only for $CsPbBr_3$ and $CsPbCl_3$. Simulations using density functional theory (DFT) are used to determine the unique effect of LiBr compared to other similar salts (e.g., LiF) that do not impact the morphology of the perovskite. LiBr is found to create a more polar surface compared to LiF and the pure perovskite surface. This polar surface enables water molecules to be absorbed into the perovskite much more easily,[42] disrupting ionic and covalent bonds. This causes high molecular mobility, dewetting and recrystallization of the film into nanostructures of higher crystalline quality. Therefore, the large-scale mass transport observed only happens when passivated perovskite films are taken out of vacuum.

2. Results and Discussion

The perovskite films are deposited through synchronous dual-source sublimation with a 1:1 ratio of $CsX:PbX_2$, a method that has shown great crystal quality and produced bright LED devices and efficient solar cells.[12–16] Lithium salt is sublimated in the same chamber from a single source. The substrate is kept at a fixed distance and rotates at a constant rate during deposition. Each salt evaporation rate was tuned to obtain the desired stoichiometric ratio. XRD measurement of the pure films confirmed the presence of well-formed $CsPbX_3$ crystal structures on relatively thick films (75 nm), orthorhombic for $CsPbBr_3$ and $CsPbCl_3$, and nonperovskite delta phase $CsPbI_3$ (Figure S1, Supporting Information). The $CsPbI_3$ delta phase was expected as the films were taken out to ambient atmosphere for the measurement and this material rapidly transitions to this phase when in contact with moisture.[17,18]

2.1. LiBr Impact on Morphology and Crystal Structure

The $CsPbX_3$ films strongly react to the deposition of only 5 Å of LiBr as seen in **Figure 1** for 5 and 15 nm films respectively. It is essential to keep in mind that the films are solid crystals before the addition of the passivation salt, which makes the transformation even more interesting. We also do not apply any annealing treatment to the perovskite to observe the impact of the lithium salt only. Like $CsPbBr_3$ which was previously demonstrated to self-assemble into islands after passivation, the LiBr-passivated $CsPbCl_3$ films also show drastic agglomeration into individual islands, even though it is known to have a more stable crystal structure than $CsPbBr_3$ with fewer phase transitions.[19,20] With a heavier element in the halide position of the perovskite, $CsPbI_3$ uniquely behaves. While still dewetting from the surface and rearranging itself, the film shows clear preferential growth orientations during the recrystallization process with triangular and rod-shaped structures, demonstrating two competing processes. A gradual increase of the LiBr amount on 5 nm films, as shown in **Figure 2**, causes the agglomerated island size to increase for $CsPbBr_3$ and $CsPbCl_3$. More lithium salt causes more bond disruption and dewetting, increasing the perovskite mobility on the surface which coalesces smaller islands into large ones following surface energy minimization. For $CsPbI_3$, the rod structures grow significantly longer when adding more LiBr, reaching above 2 µm while maintaining a ≈100 nm width, which proves the preferential direction of growth. The triangular structures do not increase in size or in number with an increase in LiBr. The reverse process of keeping the LiBr amount fixed, 5 Å, while increasing the perovskite thickness, is shown for $CsPbBr_3$ in Figure S2 in the Supporting Information. We can observe that

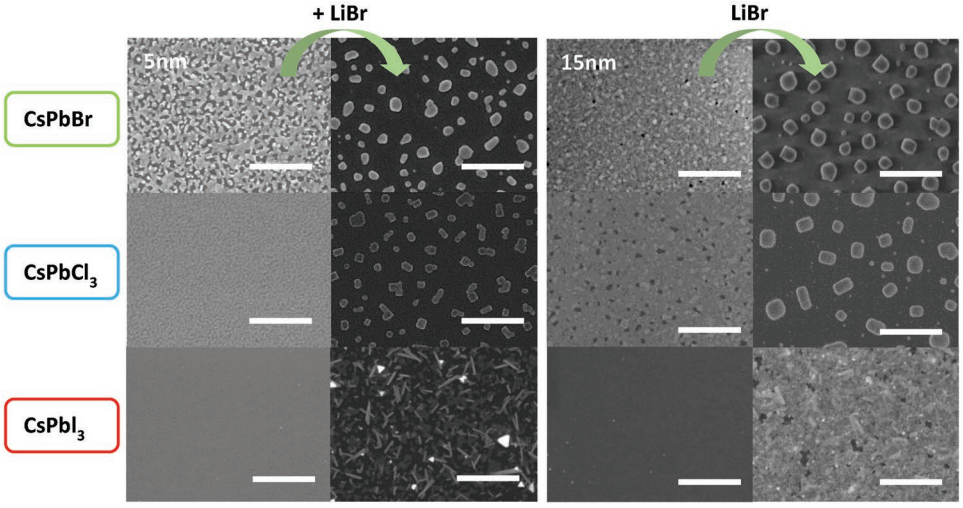

Figure 1. 5 and 15 nm films of $CsPbX_3$ (X = I, Br, Cl) with and without 5 Å LiBr deposited on top. Strong restructuration into nanostructures is observed for all films. Scale bars: 1 µm.

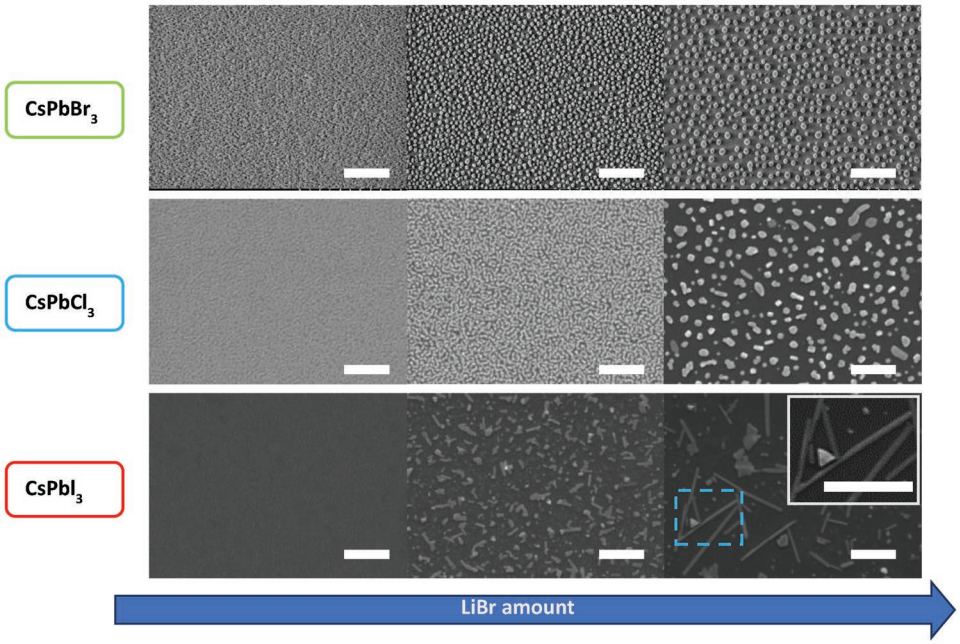

Figure 2. a) Gradual transition to nanostructures following the increase of LiBr added to the 5 nm $CsPbX_3$ films. The size of islands increases and length of the rods follows the increase of LiBr. Scale bars: 1 µm.

LiBr does not cause formation of individual islands for thickness >75 nm, as shown in **Figure 3**. The film transformation generally begins with pin-holes or voids that are created at junction points between several crystal grains. The perovskite films visually behave the same way as copper thin films do when treated to high temperature,[21,22] with the film showing weak cohesive energy, forming larger grains driven by minimizing surface energy. The 75 nm passivated films were used for XRD analysis. The $CsPbBr_3$ showed a clear new crystal structure after passivation, with the introduction of a Cs_4PbBr_6 phase in addition to the orthorhombic $CsPbBr_3$ phase (Figure S1, Supporting Information). No extra phase is observed for $CsPbCl_3$ and $CsPbI_3$, but our XRD instrument resolution limits to the use of these thicker films. We would expect to observe extra phases on thinner films with the varied nanostructures.

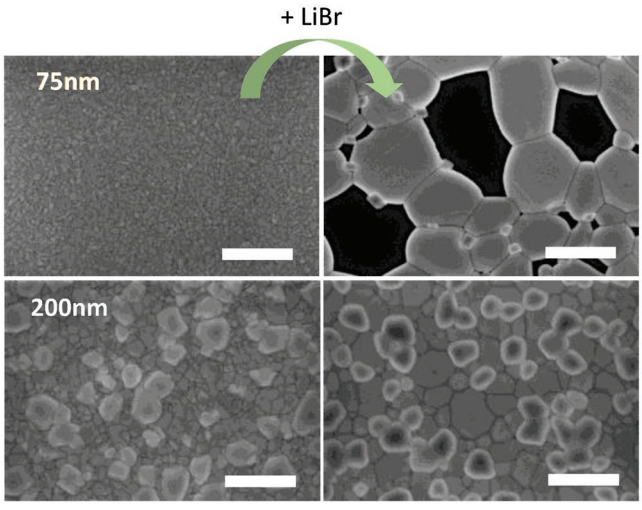

Figure 3. SEM images of thicker $CsPbBr_3$ films while maintaining a 5 Å LiBr passivation. Scale bars: 500 nm.

To confirm this hypothesis, the high-resolution TEM imaging was used to determine the structure of each 5 nm thick $CsPbX_3$. **Figure 4**a,b shows different crystal lattice spacings when comparing the triangular and the rod structure in the $CsPbI_3$. The d-spacing of 2.1 Å for triangles fits the delta-phase structure whereas the d-spacing of 3.2 Å measured of the rods indicates the emergence of an orthorhombic perovskite $CsPbI_2Br$.[23,24] The directional growth would be explained by the anisotropic structure of the $CsPbI_2Br$, with iodine centered on four faces of the crystal lattice and cesium centered on the other two. This is similar to the self-assembly of orthorhombic $CsPbI_3$ nanowires that has been previously observed with the use of polar solvents for perovskite nanocubes.[25] The adsorption of a polar molecule causes lattice distortion and therefore a polar moment that would create dipole–dipole attraction and oriented growth. The difference in crystal structure stability for $CsPbI_3$ likely explains the striking difference in final morphology after passivation. The $CsPbCl_3$ has a d-spacing of 2.8 Å corresponding to (200) plane (lattice parameter = 5.6 Å) as well the $CsPbBr_3$ sample demonstrates a d-spacing of 4.2 Å corresponding to (110) plane (lattice parameter = 5.9 Å). When analyzing the fast Fourier transform patterns (Figure S3, Supporting Information) of these two passivated films, both contain traces of hexagonal structures, Cs_4PbX_6.

The films are taken out of deposition chamber and transferred in ambient atmosphere to the SEM/TEM systems for imaging analysis. The direct contact with atmosphere can play a role in the degradation of perovskites as observed before.[26–28] $CsPbI_3$ in particular instantaneously transitions to a nonradiative delta-phase structure when in contact with humidity.[29–31]

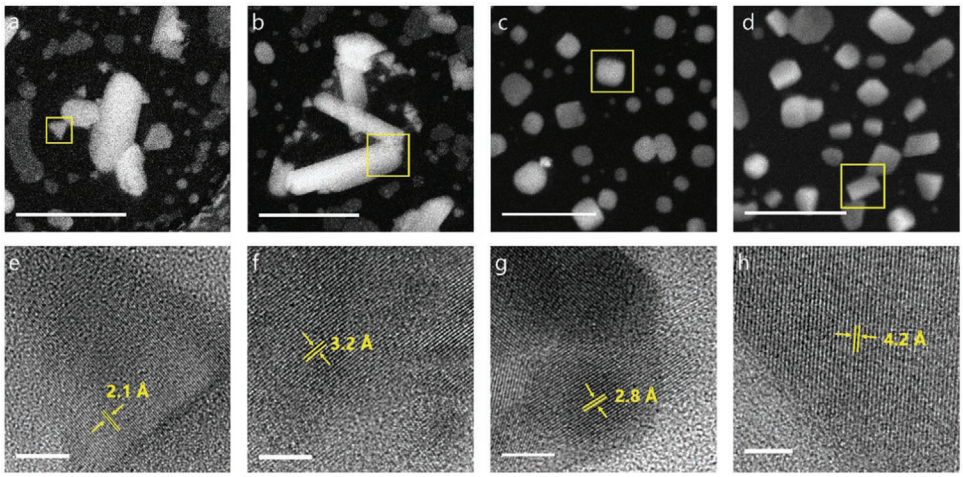

Figure 4. a–d) STEM-Z contrast (ZC) images showing the morphology of triangular $CsPbI_3$, rod-like CsPbI3, $CsPbCl_3$, and $CsPbBr_3$ nanocrystals, respectively. Scale bars: 200 nm. e,f) High resolution transfer electron microscopy images showing the lattice fringes of each corresponding nanocrystal indicated by yellow square in the STEM-ZC images. Scale bars: 5 nm. All films are of 5 nm nominal thickness.

The impact of humidity on inorganic perovskites is not always bad as humidity can help the crystallization process and brightness of the films.[32] Humid atmosphere has been used before to improve perovskite grain growth during annealing with great success.[33] To determine if humidity played a role in the morphology change of our films, pure $CsPbX_3$ films were treated to a high humidity atmosphere (60% relative humidity (RH)) for a range of time and then compared to the same films kept in dry air (20% RH) (Figures S4–S6 in the Supporting Information). We find that pure $CsPbBr_3$ and $CsPbCl_3$ films are affected by the high humidity, with a melting behavior causing dewetting on the surface and rearrangement of the continuous film in a similar fashion to the passivated films in dryer (normal) atmosphere. On the other hand, $CsPbI_3$ does not react like the other compounds when left in high humidity, even for an extended period of time. This raises the question: Why is LiBr causing such changes in dry atmosphere, even with $CsPbI_3$, and does the mass transport require contact with atmosphere to happen at all?

2.2. Surface Energy not Acting as the Catalyst

LiBr is a well-known desiccant, used for moisture absorption in refrigeration applications.[34–37] We previously tested the passivation with other lithium salts. Although LiCl has similar strong desiccant properties as LiF, **Figure 5** shows, however, that the film restructuration is observed only with LiCl but not for LiF, NaBr or KBr. A common physical reason for thin films to change morphology, or dewet from the substrate, is a disruption of the surface energy balance between the atmosphere-film-substrate interfaces. Studies on the adjustment of surface ligands showed that perovskite thin films can show liquid-like behavior following a surface energy gradient and increase grain size.[38] However, the inception of the phenomenon observed in this work cannot be attributed to a surface energy change, even if the final shape of the structures does follow surface energy minimization. As shown in Figure 5f, a DFT calculation for a $CsPbBr_3$ crystal with varied salt surface terminations shows a significant increase or decrease in surface energy compared

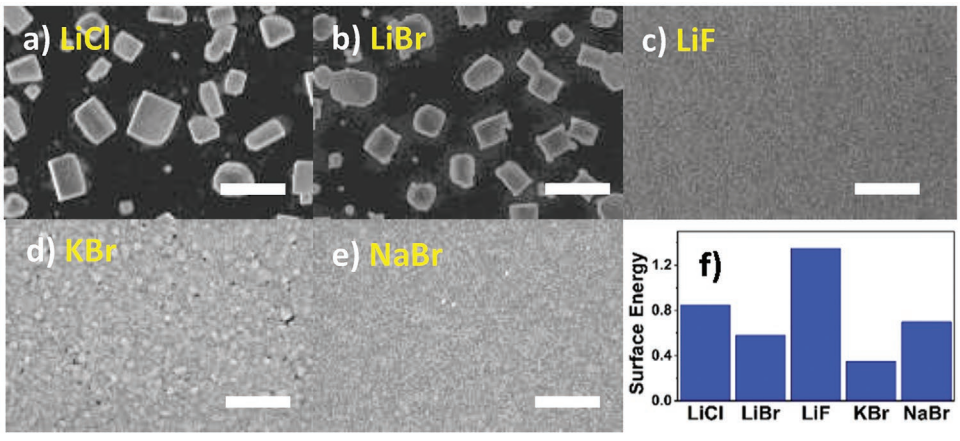

Figure 5. a–e) Impact of lithium and bromide salts on $CsPbBr_3$ 15 nm film morphology. 500 nm scale bar. f) DFT calculation of the surface energy for $CsPbBr_3$ crystal with varying salt terminations. Scale bars: 500 nm.

to LiBr, but no self-assembly is observed for these other salts. Water molecules attached to lead halide perovskites are known to cause the ionic and octahedra bonds (Pb-X in this case) to weaken.[39] This softening of the structure has been observed to create a Cs_4PbX_6-H_2O phase change.[40] The insertion of specific inorganic halide salts like CsI and RbI in perovskite films has been shown to disrupt the moisture stability and cause phase transition before.[41] The LiBr acting as a catalyst for water adsorption in the perovskite would explain the observation of the Cs_4PbBr_6 in the XRD analysis.

2.3. Role of Humidity Exposure in the Transformation

We previously observed a shift in elemental binding energy of $CsPbBr_3$ in X-ray photoelectron spectroscopy (XPS) measurements for our LiBr-passivated samples.[11] Those films were transferred, with short contact with atmosphere, from one vacuum system to another for the XPS measurements. New $CsPbBr_3$ films were created in the same vacuum system connected to the XPS and in-situ measurements were taken again before and after passivation, Figure S7 in the Supporting Information, with no noticeable energy shift after passivation. Therefore, the combination of LiBr and ambient atmosphere seems crucial in the restructuration of the perovskite film. In ambient air, at room temperature, LiBr causes these solid thin films to melt and recrystallize, improving crystallinity without any annealing treatment. The humidity treatment used in Figures S4–S6 in the Supporting Information was also applied to LiBr-passivated $CsPbBr_3$ samples that had been taken out into atmosphere (Figure S8, Supporting Information). The increased humidity exposure does not drastically change the overall morphology of already self-assembled islands, except with a slight increase of the average island size. We also compared LED pixels for which the LiBr-passivated perovskite was either exposed to atmosphere or kept in vacuum during the fabrication process before being covered with the remaining layers of the device, Figure S9 in the Supporting Information. The pixel exposed to atmosphere is uniform with no dark spots while the one fully kept in vacuum shows clear signs of deterioration with bubbles forming between layers. The LiBr-passivated perovskite has to be treated to the humidity in the ambient atmosphere otherwise the device layer structure falls apart.

2.4. DFT Computations of Water Interaction with the Perovskite Surface

DFT simulations were used to attempt to isolate the role of the lithium salt when deposited on the perovskite surface. The $CsPbBr_3$ perovskite was first relaxed as a bulk *Pm3m* cubic structure, then with the [001] surface normal direction and a Cs-Br terminating surface exposed to a 30 Å vacuum layer with three layers (15 Å) of atoms allowed to relax into the vacuum supported by two layers (9 Å) of atoms held fixed in the relaxed bulk geometry. Molecular LiX (X = Br or F) was then added on the surface to observe how the salt impacted the structural properties of the film. LiF was previously tested on perovskites and did not change the film morphology which makes it a good comparison to LiBr. SEM images of the pure LiX films, Figure S13 in the Supporting Information, indicate that the deposited salts on top of the perovskite should both be non-continuous and covering a similar area. Following the addition of the salt, the fully relaxed $CsPbBr_3$ structure is very similar between the two simulations (**Figure 6**a) with the LiX inserting itself next to Cs on top of the Pb atom. First, we can see that the cubic structure shifts to the orthorhombic phase with the typical tilted octahedra lowering the total energy of the perovskite. This is another demonstration of the cubic perovskite being a thermodynamically unstable phase which rearranges itself to orthorhombic given any stress inflicted on the structure and no confining restriction, a process well studied in the literature.[42] The simulated crystal otherwise does not show any structural or mechanical strain difference between the LiBr and the LiF-passivated surfaces. The key variation is in the charge density change on the surface induced by these salts, as shown in Figure 6b,c where isosurfaces show charge depletion (blue) or charge augmentation (white). LiF redistributes charges evenly within small radii and within the confines of the perovskite top layer with the F atom found to bond with the two neighbor Cs atoms as seen in Figure 6b. For the LiBr salt, the Br gains more charge from Li while positioning itself in continuation of the octahedra formation of the perovskite. The isosurfaces for the LiBr extend much farther beyond the surface of the perovskite, creating a polar surface for approaching water molecules. This is found to significantly increase the Van der Waals force between water molecules and the perovskite surface when compared to the pure and the LiF-passivated surfaces. The initial position of the water molecule was determined after molecular dynamic relaxation. The total energy of the system as a function of the distance of a water molecule from the LiX-$CsPbBr_3$ surface can be seen in **Figure 7**a, with the LiBr surface showing a slope directly proportional to the attractive force, which is much sharper than that of the bare and LiF surfaces, and a deeper

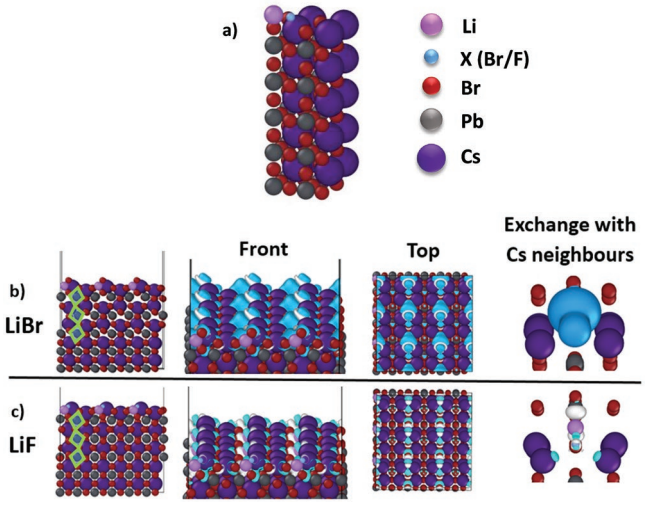

Figure 6. a) Relaxed $CsPbBr_3$ cubic structure onto which the LiX salt is added. b,c) Fully relaxed structure and charge density difference in $CsPbBr_3$ surface with added molecular b) LiBr and c) LiF (blue regions: charge decrease, white region: charge increase; same isolevel of ±0.0004 e A^{-1}). The LiF charge exchange with Cs is observed by reducing the radius scaling factor to 40% and increase the isolevel to ±0.004 e A^{-1}.

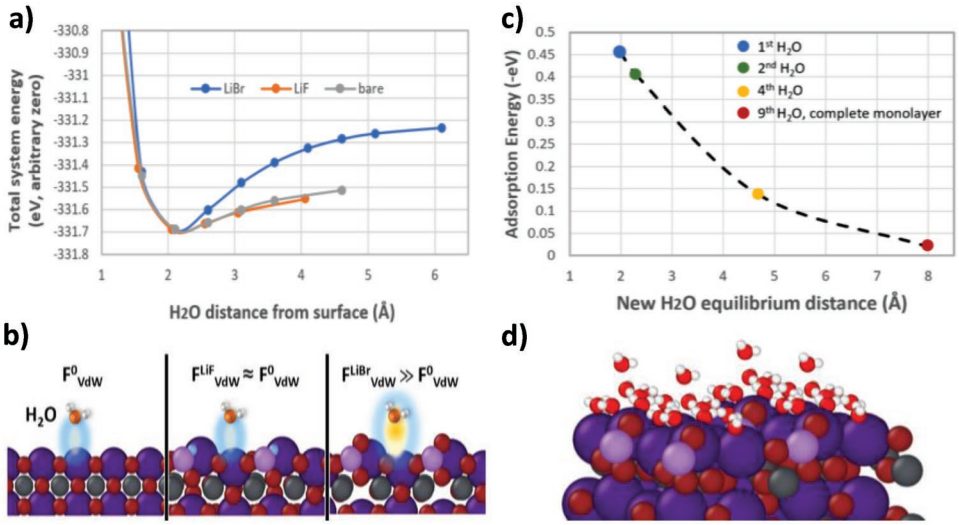

Figure 7. a) Total system energy dependence on the water molecule distance from the perovskite surface containing the LiX salt. The slope of the graph represents the force of attraction. b) Diagram for visualization of the increase of the Van der Waals attraction of water molecules for the LiBr surface compared to the pure perovskite and the LiF surface. c) Impact of the LiBr-perovskite surface water coverage on the adsorption energy and the equilibrium position of additional H_2O molecules. d) Relaxed LiBr-passivated $CsPbBr_3$ surface with 9 H_2O molecules added to the surface.

potential well. This correlates to previous studies showing that water adsorption at perovskite surfaces is known to be significantly increased if polarity is introduced to the surface.[43] It was also known that the ionic nature of metal halide perovskites makes them easily soluble in polar solvents, such as water, while ions can recrystallize if the concentration exceeds the solubility.[44] Our system would be a direct example of such a case, with the polar solvent only coming from atmospheric moisture. A polar surface on metal halide perovskites is typically found to deteriorate their luminescence efficiency, due to a decrease in exciton binding energy, an increase in trap states and corrosion of the surface.[45,46] But in a system that is allowed to relax and restructure through mass transport like our present case, the charge on the surface of the perovskite likely neutralizes and is more much stable than its initial state.

The $CsPbI_3$ self-assembled rod structures were also previously observed by leaving nanocrystals in a polar environment, whereas $CsPbBr_3$ and $CsPbCl_3$ would form individual islands.[47] In our $CsPbI_3$ samples, a self-assembly into $CsPbI_2Br$ rods also occurs but competes against the strong tendency of transition toward δ-phase in atmosphere. The $CsPbBr_3$ density of state was also calculated, shown in Figure S10 in the Supporting Information, after relaxation and did not show any shift for the perovskite with and without LiBr, which correlates with the XPS experimental data, shown in Figure S7 in the Supporting Information, for samples parked in vacuum.

The impact of increased moisture content on the surface is provided in Figure S11 in the Supporting Information. The molecular dynamic relaxation with increasing moisture shows that with increasing number of water molecules on the surface, the attractive force for an additional molecule on the perovskite decreases. Figure 7c demonstrates a clear screening effect caused by the water coverage for incoming molecules. A higher coverage decreases the magnitude of adsorption energy of new water molecules and pushes their equilibrium position farther away from the surface, as shown in Figure 7d. Consequently, the LiBr does not create a strong migration of water molecules within the perovskite but facilitates their capture on the surface. Until the structure is ruptured by ionization and creates more area for the water to interact with the surface, the water does not increasingly diffuse into the perovskite.

We therefore conclude that the perovskite films do not instantaneously restructure and recrystallize when in contact with the LiBr but do so when the $LiBr \cdot CsPbX_3$ surface is in contact with moisture. While VPD methods for perovskite fabrication have a lot of advantages, this work demonstrates the delicate care needed in adjusting the device fabrication process when introducing a passivation agent in vacuum. Atmosphere or controlled moisture exposure for the perovskite film can be beneficial as an annealing process to improve crystallinity and lower defects but has to be accomplished before additional device layers are deposited.

3. Conclusion

In summary, we have shown the drastic mass transport and restructuration happening in VPD $CsPbX_3$ films after LiBr passivation. $CsPbBr_3$ and $CsPbCl_3$ are self-assembled into islands while $CsPbI_3$ was found to transform into triangular and rod-shaped nanostructures. The increase of LiBr leads to an increase in the size of islands for $CsPbBr_3$ and $CsPbCl_3$ and elongated rods for $CsPbI_3$. A new Cs_4PbBr_6 phase was observed after passivation, attributed to the insertion of moisture in the crystal. The perovskites were found to react similarly to high humidity atmosphere except for $CsPbI_3$, which maintains its stable delta-phase continuous film. Through TEM imaging analysis, we observed orthorhombic $CsPbI_3$ perovskite rods. DFT simulations show that the LiBr plays a unique role of creating a polar surface facilitating water adsorption without altering the crystal structure. The self-assembly phenomenon for the $CsPbX_3$ films is therefore not attributed to LiBr passivation by itself, but the

subsequent interaction with water molecules. This information is important when devising VPD fabrication protocols as passivated perovskite films, if not treated beforehand, can wreck the delicate structural integrity of optoelectronic devices.

4. Experimental Section

The $CsPbX_3$ films were deposited via dual-source thermal coevaporation with a fixed molar ratio and flux ratio of CsX and PbX_2 at 1:1. The ratio was measured by the PHI 5500 Multi-Technique XPS system to provide a feedback on the stoichiometry of the film. The thickness and deposition rates of films were monitored by two quartz crystal microbalances. All the depositions were done in vacuum at a pressure below 2×10^{-4} Pa, with the substrate kept at room temperature. LiBr and other halide salts were deposited in the same chamber under the same vacuum conditions. All materials were obtained in powder form from Sigma-Aldrich, with a purity >99%. It is important to note that there was no annealing treatment of any kind on the material. Before deposition, all sources were degassed at slightly lower temperature than their respective sublimation/evaporation temperature for at least an hour.

Morphological information was obtained by using a scanning transmission electron microscope (STEM) (Hitachi HF 3300) and a scanning electron microscope (Hitachi S5200). X-ray Diffraction analysis was accomplished with the Rigaku Miniflex 600 with the perovskite films on rotating Si wafers. Density functional theory was used to calculate surface energy of various salt-passivated perovskites and simulate the water interaction with the perovskite surface.[48–50] More details are included in the Supporting Information regarding the computations.

Supporting Information

Supporting Information is available from the Wiley Online Library or from the author.

Acknowledgements

The financial support for the work in this paper was provided by Canada Research Chair in Organic Optoelectronics (Zheng-Hong Lu, grant number 950-220944) and the Natural Science and Engineering Research Council of Canada (NSERC, grant numbers 216956-12 and RGPIN-2018-04642). Computational resources were provided by Compute Canada.

Conflict of Interest

The authors declare no conflict of interest.

Data Availability Statement

The data that support the findings of this study are available from the corresponding author upon reasonable request.

Keywords

mass transport, passivation, perovskite, thermal evaporation

Received: June 10, 2022
Revised: July 28, 2022
Published online: September 9, 2022

[1] Y. Zu, J. Dai, L. Li, F. Yuan, X. Chen, Z. Feng, K. Li, X. Song, F. Yun, Y. Yu, B. Jiao, *J. Mater. Chem. A* **2019**, *7*, 26116.
[2] Y. M. Chen, Y. Zhou, Q. Zhao, J. Y. Zhang, J. P. Ma, T. T. Xuan, S. Q. Guo, Z. J. Yong, J. Wang, Y. Kuroiwa, C. Moriyoshi, *ACS Appl. Mater. Interfaces* **2018**, *10*, 15905.
[3] Z. K. Zhou, Z. H. Mo, X. L. Wei, *Chem. Commun.* **2019**, *55*, 11916.
[4] W. Zhou, Y. Zhao, E. Wang, Q. Li, S. Lou, J. Wang, X. Li, Q. Lian, Q. Xie, R. Q. Zhang, H. Zeng, *J. Phys. Chem. Lett.* **2020**, *11*, 3159.
[5] K. Zhang, N. Zhu, M. Zhang, L. Wang, J. Xing, *J. Mater. Chem. C* **2021**, *9*, 3795.
[6] N. Wang, L. Cheng, R. Ge, S. Zhang, Y. Miao, W. Zou, C. Yi, Y. Sun, Y. Cao, R. Yang, Y. Wei, Q. Guo, Y. Ke, M. Yu, Y. Jin, Y. Liu, Q. Ding, D. Di, L. Yang, G. Xing, H. Tian, C. Jin, F. Gao, R. H. Friend, J. Wang, W. Huang, *Nat. Photonics* **2016**, *10*, 699.
[7] P. Du, J. Li, L. Wang, L. Sun, X. Wang, X. Xu, L. Yang, J. Pang, W. Liang, J. Luo, Y. Ma, J. Tang, *Nat. Commun.* **2021**, *12*, 4751.
[8] J. Zhao, M. Liu, L. Fang, S. Jiang, J. Zhou, H. Ding, H. Huang, W. Wen, Z. Luo, Q. Zhang, X. Wang, *J. Phys. Chem. Lett.* **2017**, *8*, 3115.
[9] Y. Zhao, Y. Wang, J. Duan, X. Yang, Q. Tang, *J. Mater. Chem. A* **2019**, *7*, 6877.
[10] T. Wu, J. Li, Y. Zou, H. Xu, K. Wen, S. Wan, S. Bai, T. Song, J. A. McLeod, S. Duhm, F. Gao, *Angew. Chem., Int. Ed.* **2020**, *59*, 4099.
[11] A. Dumont, K. Ho, H. T. Kung, C. Qiu, P. Li, D. Luo, Y. Zhao, G. Walker, Z. H. Lu, *Adv. Mater. Interfaces* **2020**, *7*, 2000506.
[12] J. Ávila, C. Momblona, P. P. Boix, M. Sessolo, H. J. Bolink, *Joule* **2017**, *1*, 431.
[13] Y. Hu, Q. Wang, Y.-L. Shi, M. Li, L. Zhang, Z.-K. Wang, L.-S. Liao, *J. Mater. Chem. C* **2017**, *5*, 8144.
[14] Q. Ma, S. Huang, X. Wen, M. A. Green, A. W. Ho-Baillie, *Adv. Energy Mater.* **2016**, *6*, 1502202.
[15] J. Lei, F. Gao, H. Wang, J. Li, J. Jiang, X. Wu, R. Gao, Z. Yang, S. F. Liu, *Sol. Energy Mater. Sol. Cells* **2018**, *187*, 1.
[16] J. M. Ball, L. Buizza, H. C. Sansom, M. D. Farrar, M. T. Klug, J. Borchert, J. Patel, L. M. Herz, M. B. Johnston, H. J. Snaith, *ACS Energy Lett.* **2019**, *4*, 2748.
[17] K. Ho, M. Wei, E. H. Sargent, G. C. Walker, *Optical Devices and Materials for Solar Energy and Solid-State Lighting*, Optical Society of America, Montreal, **2021**, p. PvM2B-3.
[18] E. Breniaux, P. Dufour, S. Guillemet-Fritsch, C. Tenailleau, *Eur. J. Inorg. Chem.* **2021**, *2021*, 3059.
[19] S. Hirotsu, *J. Phys. Soc. Jpn.* **1971**, *31*, 552.
[20] M. Hidaka, Y. Okamoto, Y. Zikumaru, *Phys. Status Solidi A* **1983**, *79*, 263.
[21] D. Sonawane, P. Kumar, *Nanotechnology* **2021**, *32*, 195703.
[22] J. Gao, A. Malchère, S. Yang, A. Campos, T. Luo, K. Quertite, P. Steyer, C. Girardeaux, L. Zhang, D. Mangelinck, *Acta Mater.* **2022**, *223*, 117491.
[23] C. K. Møller, *Mat. Fys. Medd. Dan. Vid. Selsk. Munksgaard* **1959**, *32*, 1.
[24] S. Ullah, J. Wang, P. Yang, L. Liu, Y. Li, S. E. Yang, T. Xia, H. Guo, Y. Chen, *Energy Technol.* **2021**, *9*, 2100691.
[25] J. K. Sun, S. Huang, X. Z. Liu, Q. Xu, Q. H. Zhang, W. J. Jiang, D. J. Xue, J. C. Xu, J. Y. Ma, J. Ding, Q. Q. Ge, *J. Am. Chem. Soc.* **2018**, *140*, 11705.
[26] T. Leijtens, E. T. Hoke, G. Grancini, D. J. Slotcavage, G. E. Eperon, J. M. Ball, M. De Bastiani, A. R. Bowring, N. Martino, K. Wojciechowski, M. D. McGehee, *Adv. Energy Mater.* **2015**, *5*, 1500962.
[27] C. X. Zhang, T. Shen, D. Guo, L. M. Tang, K. Yang, H. X. Deng, *InfoMat* **2020**, *2*, 1034.
[28] M. I. Saidaminov, J. Kim, A. Jain, R. Quintero-Bermudez, H. Tan, G. Long, F. Tan, A. Johnston, Y. Zhao, O. Voznyy, E. H. Sargent, *Nat. Energy* **2018**, *3*, 648.

[29] G. Yuan, C. Ritchie, M. Ritter, S. Murphy, D. E. Gómez, P. Mulvaney, *J. Phys. Chem. C* **2017**, *122*, 13407.
[30] Z. Li, M. Yang, J. S. Park, S. H. Wei, J. J. Berry, K. Zhu, *Chem. Mater.* **2016**, *28*, 284.
[31] C. C. Boyd, R. Cheacharoen, T. Leijtens, M. D. McGehee, *Chem. Rev.* **2018**, *119*, 3418.
[32] D. Di Girolamo, M. I. Dar, D. Dini, L. Gontrani, R. Caminiti, A. Mattoni, M. Graetzel, S. Meloni, *J. Mater. Chem. A* **2019**, *7*, 12292.
[33] J. You, Y. Yang, Z. Hong, T. B. Song, L. Meng, Y. Liu, C. Jiang, H. Zhou, W. H. Chang, G. Li, Y. Yang, *Appl. Phys. Lett.* **2014**, *105*, 183902.
[34] R. D. Misra, P. K. Sahoo, S. Sahoo, A. Gupta, *Int. J. Refrig.* **2003**, *26*, 158.
[35] W. B. Ma, S. M. Deng, *Int. J. Refrig.* **1996**, *19*, 141.
[36] R. Maryami, A. A. Dehghan, *Appl. Therm. Eng.* **2017**, *124*, 103.
[37] M. A. Hammad, M. S. Audi, *Renewable Energy* **1992**, *2*, 275.
[38] J. Xue, R. Wang, K. L. Wang, Z. K. Wang, I. Yavuz, Y. Wang, Y. Yang, X. Gao, T. Huang, S. Nuryyeva, J. W. Lee, *J. Am. Chem. Soc.* **2019**, *141*, 13948.
[39] L. Zhang, M. G. Ju, W. Liang, *Phys. Chem. Chem. Phys.* **2016**, *18*, 23174.
[40] M. Shin, S. W. Nam, A. Sadhanala, R. Shivanna, M. Anaya, A. Jimenez-Solano, H. Yoon, S. Jeon, S. D. Stranks, R. L. Hoye, B. Shin, *ACS Appl. Energy Mater.* **2019**, *3*, 192.
[41] Y. Hu, M. F. Aygüler, M. L. Petrus, T. Bein, P. Docampo, *ACS Energy Lett.* **2017**, *2*, 2212.
[42] J. S. Bechtel, J. C. Thomas, A. Van der Ven, *Phys. Rev. Mater.* **2019**, *3*, 113605.
[43] N. Z. Koocher, D. Saldana-Greco, F. Wang, S. Liu, A. M. Rappe, *J. Phys. Chem. Lett.* **2015**, *6*, 4371.
[44] P. Lu, M. Lu, H. Wang, N. Sui, Z. Shi, W. W. Yu, Y. Zhang,, *InfoMat* **2019**, *1*, 430.
[45] H. Lian, Y. Li, S. Saravanakumar, H. Jiang, Z. Li, J. Wang, L. Xu, W. Zhao, G. Han, *Coord. Chem. Rev.* **2022**, *452*, 214313.
[46] C. Ma, D. Shen, J. Qing, H. Thachoth Chandran, M. F. Lo, C. S. Lee, *ACS Appl. Mater. Interfaces* **2017**, *9*, 14960.
[47] T. Udayabhaskararao, M. Kazes, L. Houben, H. Lin, D. Oron, *Chem. Mater.* **2017**, *29*, 1302.
[48] G. Kresse, J. Furthmüller, *Phys. Rev. B* **1996**, *54*, 11169.
[49] G. Kresse, D. Joubert, *Phys. Rev. B* **1999**, *59*, 1758.
[50] J. P. Perdew, K. Burke, M. Ernzerhof, *Phys. Rev. Lett.* **1996**, *77*, 3865.